# Functional Analysis of γ-Tubulin Complex Proteins Indicates Specific Lateral Association via Their N-terminal Domains

Dorian Farache, Alain Jauneau, Cécile Chemin, Marine Chartrain, Marie-Hélène Rémy, Andreas Merdes, Laurence Haren

THE JOURNAL OF BIOLOGICAL CHEMISTRY VOL. 291, NO. 44, pp. 23112–23125, October 28, 2016


# Functional Analysis of γ-Tubulin Complex Proteins Indicates Specific Lateral Association via Their N-terminal Domains*

Received for publication, June 22, 2016, and in revised form, September 20, 2016 Published, JBC Papers in Press, September 22, 2016, DOI 10.1074/jbc.M116.744862

**Dorian Farache[‡], Alain Jauneau[§], Cécile Chemin[‡], Marine Chartrain[‡1], Marie-Hélène Rémy[‡], Andreas Merdes[‡2], and Laurence Haren[‡3]**

*From the [‡]Centre de Biologie du Développement, CNRS-Université Toulouse III, 31062 Toulouse, France and [§]Plateforme Imagerie-Microscopie, FR 3450 Pôle de Biotechnologie Végétale, 31326 Castanet-Tolosan, France*

**Edited by Velia Fowler**

**Microtubules are nucleated from multiprotein complexes containing γ-tubulin and associated γ-tubulin complex proteins (GCPs). Small complexes (γTuSCs) comprise two molecules of γ-tubulin bound to the C-terminal domains of GCP2 and GCP3. γTuSCs associate laterally into helical structures, providing a structural template for microtubule nucleation. In most eukaryotes γTuSCs associate with additional GCPs (4, 5, and 6) to form the core of the so-called γ-tubulin ring complex (γTuRC). GCPs 2–6 constitute a family of homologous proteins. Previous structural analysis and modeling of GCPs suggest that all family members can potentially integrate into the helical structure. Here we provide experimental evidence for this model. Using chimeric proteins in which the N- and C-terminal domains of different GCPs are swapped, we show that the N-terminal domains define the functional identity of GCPs, whereas the C-terminal domains are exchangeable. FLIM-FRET experiments indicate that GCP4 and GCP5 associate laterally within the complex, and their interaction is mediated by their N-terminal domains as previously shown for γTuSCs. Our results suggest that all GCPs are incorporated into the helix via lateral interactions between their N-terminal domains, whereas the C-terminal domains mediate longitudinal interactions with γ-tubulin. Moreover, we show that binding to γ-tubulin is not essential for integrating into the helical complex.**

In all eukaryotes, microtubules are nucleated from specialized multiprotein complexes containing γ-tubulin and associated proteins (1–3). These complexes resemble small rings by electron microscopy and are thus called γ-tubulin ring complexes (γTuRCs)[4] (4–7). Closer inspection revealed that these γTuRCs are helices of one turn, with the two ends overlapping. They are ubiquitous and essential for viability: the growth of new microtubules is crucial to drive mitotic spindle formation and cell division.

γTuRCs are mainly composed of γ-tubulin and of proteins of the GCP (γ-tubulin complex protein) family. GCPs are characterized by sequence homology in two specific regions, also referred to as the grip1 and grip2 motifs (8). Five members of this family are known: GCPs 2, 3, 4, 5, and 6. GCPs 2 and 3 associate with γ-tubulin to form a V-shaped subcomplex, called γ-tubulin small complex (γTuSC). GCPs 2 and 3 constitute the arms of the V, interacting laterally via their N-terminal domains (Fig. 1, *A* and *B*). The C-terminal domains are located at the two tips of the V, each binding one molecule of γ-tubulin (9). In the budding yeast *Saccharomyces cerevisiae*, γTuSCs are directly recruited to the spindle pole body (yeast centrosome equivalent) by the protein Spc110. Oligomers of Spc110 interact with the basis of the V-shaped γTuSCs and stabilize their lateral association (10–13). Likely, seven γTuSCs assemble stepwise into a helix of one turn plus a small overlap (14). In this helical array, the γ-tubulin molecules are exposed to form a platform from which α/β-tubulin dimers assemble into protofilaments. The structure of these helical complexes predefines the geometry of the microtubule, with a diameter of 25 nm and with 13 γ-tubulin molecules per turn. *S. cerevisiae* represents the simplest model organism for microtubule nucleation, building γ-tubulin complexes from γTuSCs in the absence of GCPs 4, 5, and 6. In most other eukaryotes, however, GCPs 4, 5, and 6 are an integral part of γTuRCs, albeit only one or very few copies of each protein are associated with each ring (7, 8, 15–19). In human cells, preformed, inactive γTuRCs are in a soluble pool in the cytoplasm from which they are recruited to nucleation centers followed by their activation. Depletion of GCPs 4, 5 or 6 prevents the formation of stable, full-sized γTuRCs and prevents the targeting of γ-tubulin to the centrosome and to spindle microtubules (20–22). This causes errors in centriole duplication and spindle assembly, often inducing monopolar spindles (21). These phenotypes resemble defects from impaired recruitment or function of γ-tubulin (23–25).

The role of GCPs 4, 5, and 6 in γTuRC assembly is not well understood. Original observations by electron microscopy suggested that they could form a scaffolding cap at the base of the γTuSC helix (6, 7, 26). More recent structural data have challenged this model. Resolution of the atomic structure of GCP4

* This work was supported in part by Agence Nationale de la Recherche (ANR, France) Grants 08-BLAN-0281 and 13-BSV8–0007-01 and Fondation ARC pour la Recherche sur le Cancer Grant SFI20121205511. The authors declare that they have no conflicts of interest with the contents of this article.
[1] Present address: Syntivia, Oncopôle, 31106 Toulouse, France.
[2] To whom correspondence may be addressed: Centre de Biologie du Développement, CNRS-Université Toulouse III, 118 route de Narbonne, 31062 Toulouse, France. Tel.: 33-5-61-55-82-65; Fax: 33-61-55-69-52; E-mail: andreas.merdes@univ-tlse3.fr.
[3] To whom correspondence may be addressed: Centre de Biologie du Développement, CNRS-Université Toulouse III, 118 route de Narbonne, 31062 Toulouse, France. Tel.: 33-5-61-55-84-83; Fax: 33-61-55-69-52; E-mail: laurence.haren@univ-tlse3.fr.
[4] The abbreviations used are: γTuRC, γ-tubulin ring complex; GCP, γ-tubulin complex protein; γTuSC, γ-tubulin small complex; FLIM, fluorescence lifetime imaging; Nlp, ninein-like protein; CI, confidence interval.

has revealed a remarkable conservation with the structures of GCP2 and GCP3 of *S. cerevisiae*. Cryo-EM reconstructions of γTuSC helices and *in silico* modeling has shown that the atomic structure of GCP4 can be fitted into the helical wall in the place of GCPs 2 or 3 (11, 27, 28). In addition, biochemical experiments showed that GCP4 interacts with γ-tubulin via its C-terminal domain, as previously shown for GCP2 and GCP3 (9, 10, 27). *Drosophila* GCPs 5 and 6 were also found to bind γ-tubulin (29). These results led to the prediction that GCPs 4, 5, and 6 integrate into γTuRCs in an equivalent manner to GCPs 2 and 3. In this model, all GCPs would interact laterally via their N-terminal domains. Longitudinal interactions would bind γ-tubulin molecules to the C-terminal domains of each GCP (1). To test this idea experimentally, we have compared the function of the N- and C-terminal domains of GCPs 4, 5, and 6 to the equivalent domains of GCPs 2 and 3, and we have performed FLIM-FRET analysis to determine the mode of interaction between GCPs 4 and 5. We have found that the N-terminal domains define the identity of the GCP, driving lateral interactions similar to the interactions found in γTuSCs. This is the first experimental approach supporting that GCPs 4, 5, and 6 are part of the helical wall of the γTuRC.

## Results

*The Particular Role of Each GCP Is Specified by Its N-terminal Domain*—The atomic structure of GCP4 shows that the protein contains two independent domains corresponding to the N-terminal and C-terminal halves (Fig. 1*A*). All GCP proteins possess structural similarities in their N- and C-terminal domains, highlighted in *dark blue* and *red* in Fig. 1*B* (27). Nevertheless, depletion of any individual GCP from cells reduces the amount of γTuRCs and leads to mitotic defects, suggesting that the various GCPs are not functionally redundant (19–21). To investigate potential functional differences between the protein domains of individual GCPs, we developed an assay involving RNA silencing of specific GCPs and rescuing function by the expression of siRNA-resistant chimeric proteins. Our experimental setup involved stable transfection of GCP constructs into HeLa cells, taking advantage of the Flip-in T-Rex system that allows site-specific integration and inducible expression of the transgenes. To validate the system, we first verified that expression of WT GCP4 was able to rescue the depletion of the endogenous protein. We transfected an siRNA targeting GCP4 with induction of a siRNA-resistant construct at levels similar to the endogenous protein (Fig. 1*C*). Under these conditions, we measured the amount of soluble γTuRCs and their recruitment to spindles in mitosis using γ-tubulin as a marker (Fig. 1, *D–F*). In sucrose gradients, the percentage of γ-tubulin sedimenting as γTuRCs was quantified relative to total γ-tubulin levels (because the siRNA treatments delayed cell growth, total amounts of proteins varied depending on the condition) (Fig. 1, *D* and *E*). Depletion of GCP4 drastically reduced the amount of γTuRCs, whereas concomitant induction of the siRNA-resistant GCP4 restored the full-sized complexes. Depletion also reduced the recruitment of γ-tubulin to mitotic centrosomes and to spindle microtubules, which was rescued by siRNA-resistant GCP4 (Fig. 1*F*).

In a second step cells expressing chimeric proteins were analyzed. In these proteins, the N-terminal or the C-terminal domain of GCP4 was replaced by the corresponding domain of another GCP, *i.e.* 2, 3, 5, or 6 (Fig. 2). The atomic structure of GCP4 shows that the two domains are connected at a central "hinge," located between helices α11 and α12 (Fig. 1, *A* and *B*). The location of the hinge in different GCPs was determined by multiple sequence alignments (Fig. 1*B*) and was chosen as a site of recombination for the construction of chimeras. Sucrose gradient analysis showed that all chimeras carrying the N-terminal domain of GCP4 were able to rescue γTuRC formation after depletion of the endogenous GCP4 irrespective of the origin of the C-terminal domain to which they were fused (Fig. 2*A*). In contrast, chimeras with the C-terminal domain of GCP4 fused to the N-terminal domain of any other GCP failed to rescue γTuRC formation after depletion of GCP4 (Fig. 2*B*). In general, the chimeras were able to rescue only if they carried the N-terminal domain identical to the depleted endogenous GCP (Fig. 2, *A* and *B*). Quantification of γ-tubulin levels showed that rescue-competent chimeras restored nearly fully the original amounts of γTuRCs (Fig. 2*C*). They also rescued the recruitment of γ-tubulin in mitosis (Fig. 3*A*). The results are summarized in Fig. 3*B*. Occasionally, chimeras were expressed at very low levels, leading to ambiguous answers (marked with ? in Fig. 3*B*; expression levels are presented in Fig. 4). In particular, insufficient expression might explain why the chimera carrying the N-terminal domain of GCP3 does not rescue the depletion of GCP3. Alternatively, GCP3 might behave differently from the other GCPs and require its own C-terminal domain to function. Successful rescue also diminished the amount of aberrant, monopolar spindles (Fig. 3*C*), suggesting that not only the structure but also the function of γTuRCs was restored. The results show that the N-terminal domains define the functional identity of the different GCPs, whereas the C-terminal domains are exchangeable.

*GCP4 and GCP5 Are Associated Laterally via Their N-terminal Domains*—Whereas lateral interaction between the N-terminal domains of GCP2 and GCP3 has been shown previously (9, 10, 30), experimental evidence is missing on how GCPs 4, 5, and 6 bind to the remainder of the γTuRC. Modeling of the GCP4 structure into reconstructions of γTuSCs from cryo-electron microscopy has strongly suggested that GCP4 is capable of interacting laterally with other GCPs, equivalent to GCPs 2 and 3. However, this has never been verified by any biochemical or biophysical experiments. To determine whether GCP4 is involved in lateral interactions, we performed FLIM-FRET analysis. Co-immunoprecipitation experiments in *Schizosaccharomyces pombe* have suggested that GCP4 and GCP5 can bind to each other independently of γTuSCs (17). We co-expressed GCP4 and GCP5 tagged with GFP and mCherry and looked for energy transfer between the fluorescent proteins incorporated into γTuRCs at centrosomes. If the two proteins interact, the transfer of energy from the donor (GFP) to the acceptor (mCherry) decreases the fluorescence lifetime of the donor. The relative difference of lifetime is a measure of FRET efficiency and depends on the distance between the donor and the acceptor. Initial attempts of expressing fluorescent GCPs in cell lines yielded centrosomal fluorescence that was too weak

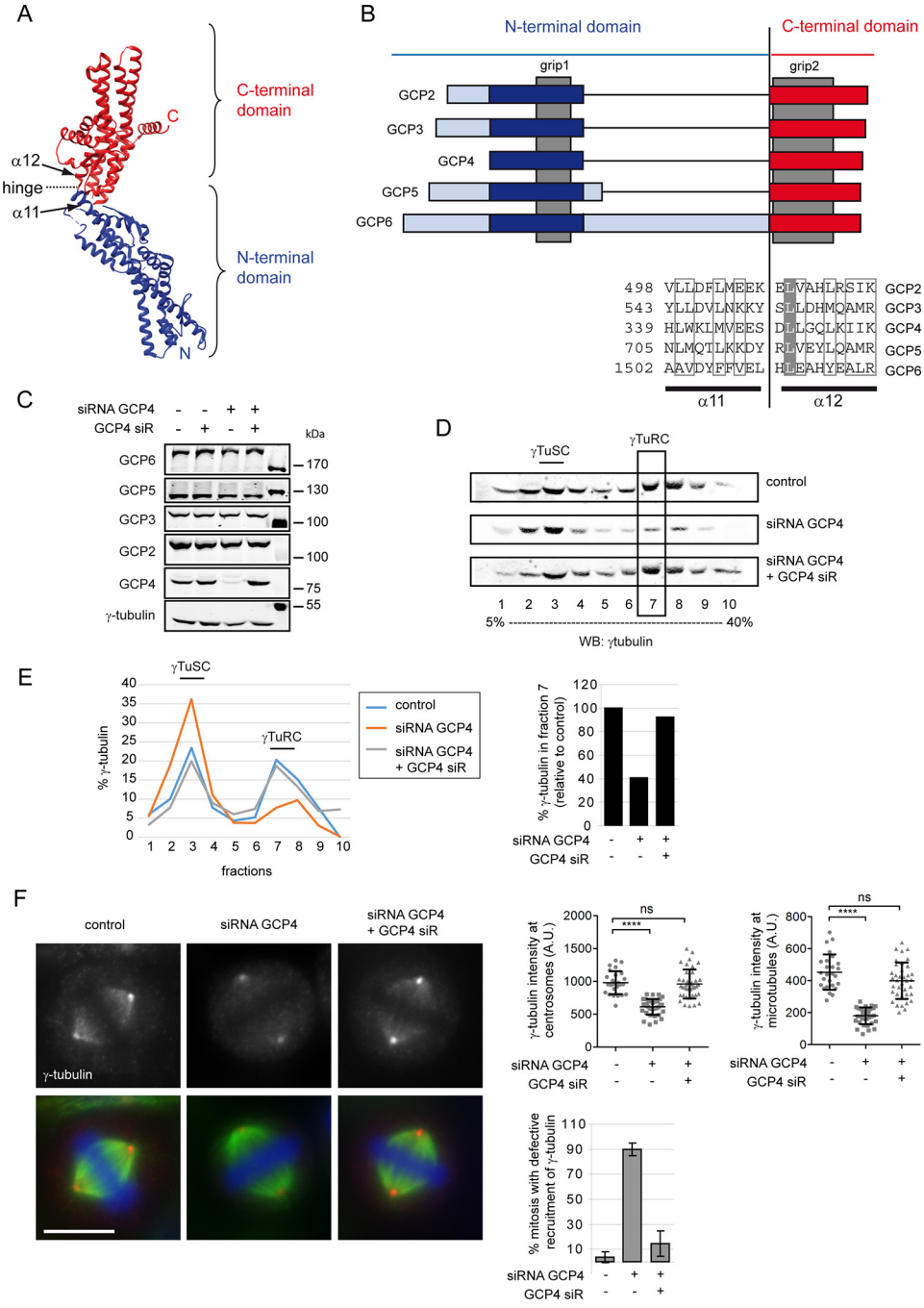


FIGURE 1. **Construction of chimeric GCPs based on GCP4 structure and rescue of GCP4 depletion phenotypes.** *A*, ribbon representation of the atomic structure of human GCP4 with the N-terminal domain delineated in *blue* and the C-terminal domain in *red*. *B*, schematic alignment of the primary structures of the five GCPs. The grip motifs are *boxed in dark gray*, the N-terminal domains are in *blue* with the specific regions in *light blue*, the C-terminal domains are in *red*. The sequences at the chimeric junction are shown relative to GCP4 helices α11 and α12. *C*, Western blot analysis of GCPs expression in HeLa cells treated with or without GCP4 siRNA with or without induction of the rescue construct resistant to the siRNA (*GCP4 siR*). *D*, comparison of extracts from control cells and cells treated with GCP4 siRNA with or without induction of GCP4 siR after fractionation in gradients of 5–40% sucrose. γTuRC sedimentation is visualized using a γ-tubulin antibody; fraction 3 contains the majority of γTuSCs, fraction 7 contains the majority of γTuRCs. *WB*, Western blot. *E*, quantification of γ-tubulin intensities in the fractions of the gels shown in *D*, expressed as a percentage of total γ-tubulin (sum of the 10 fractions). The values in fraction 7 are shown on the *right*, relative to control cells. *F*, comparison of mitosis in control cells or siRNA-treated cells with or without induction, stained for γ-tubulin (*top panels* and *red*), microtubules (*green*), and DNA (*blue*). *Scale bar*, 10 μm. *Top right*, quantification of γ-tubulin intensities at centrosomes and along spindle microtubules (>25 cells scored per condition; *error bars*, mean ± S.D.). *Bottom right*, percentage of cells with defective recruitment of γ-tubulin (mean of five experiments, 500 total cells scored per condition; *error bars*, S.E., 95% confidence interval). *ns*, not significant; ****, $p < 0.0001$.

for measuring fluorescence lifetimes. To circumvent this problem, we used a previously established cell line stably overexpressing ninein-like protein (Nlp) (31). Increased amounts of Nlp form large centrosomal assemblies in interphase that enrich γTuRCs and thereby boost microtubule nucleation. We verified by immunofluorescence that these assemblies recruit all different endogenous GCPs (Fig. 5*A*). Moreover, depletion of GCP4 or GCP5 blocked the recruitment of the other GCPs to these centrosomal assemblies, indicating that GCPs are incorporated only in the form of γTuRCs (Fig. 5*B* and data not shown).

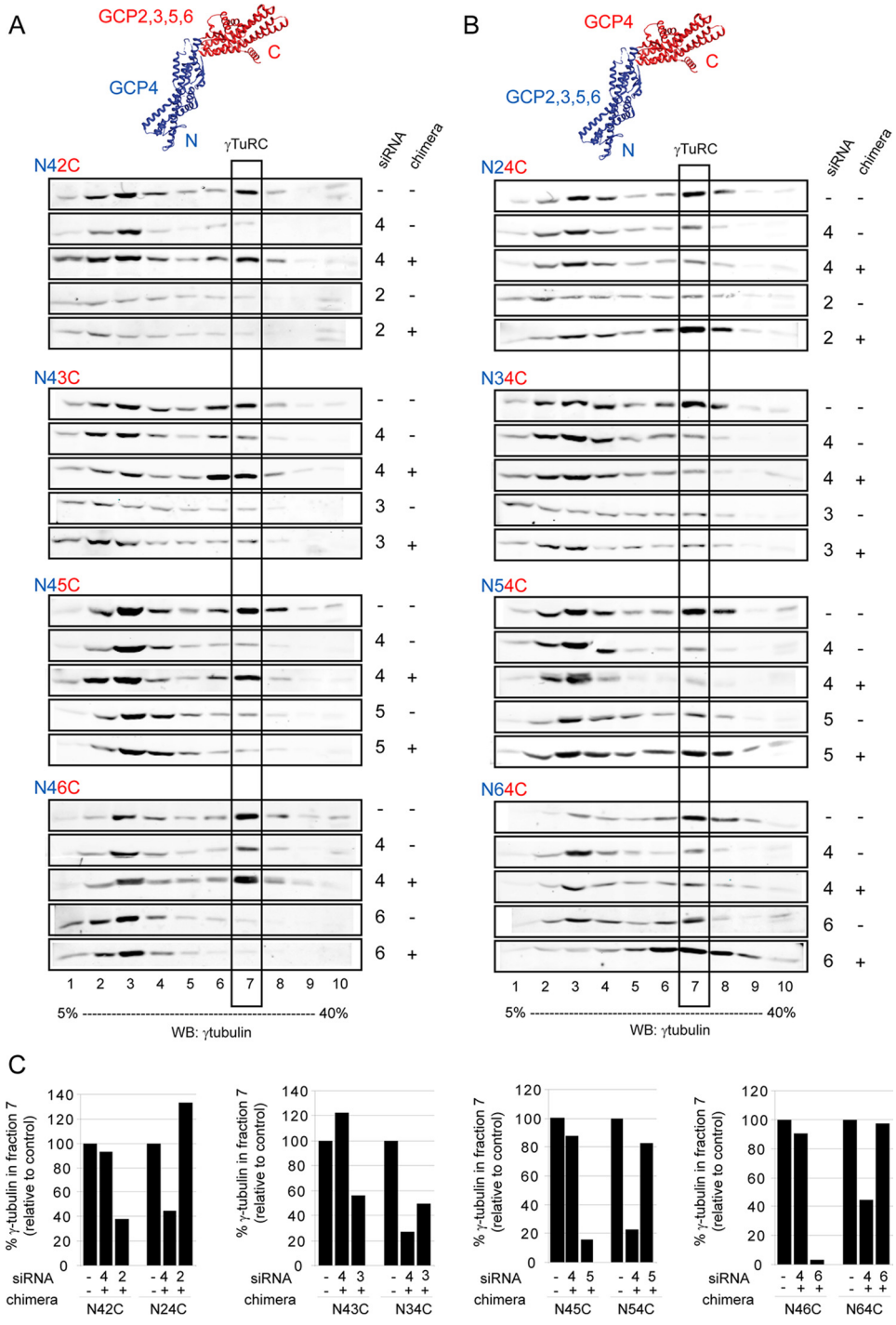


FIGURE 2. **Chimeric GCPs rescue γTuRC assembly only if they carry the N-terminal domain corresponding to the depleted GCP.** Shown is sucrose gradient fractionation of extracts from stable cell lines expressing the chimeras after depletion of the GCPs corresponding to the N- or the C-terminal domain of the chimera. *A*, chimeras composed of the N-terminal domain of GCP4 fused to the C-terminal domains of GCP 2, 3, 5, or 6 (respectively, N42C, N43C, N45C, and N46C). *B*, chimeras composed of the C-terminal domain of GCP4 fused to the N-terminal domains of GCP 2, 3, 5, or 6 (respectively, N24C, N34C, N54C, and N64C). γTuRC sedimentation is visualized using a γ-tubulin antibody. *C*, percentage of γ-tubulin in fraction 7 of the gels shown in *A* and *B*; values of siRNA-treated cells, with induction of the chimeras, are shown relative to control cells.

Our approach was designed to monitor FRET only between adjacent proteins within γTuRCs. Using the fitting models of GCP4 structure into the γTuSC helix, we predicted the distances between the extremities of the GCPs (11, 28). Because of the V-shape of γTuSCs, the N termini of adjacent GCP4 molecules were found in close contact (<2.5 nm), but the C termini were separated by an average of 6 nm. The distances between non-adjacent C termini exceeded 11 nm. As energy transfer is only possible if the distance between the fluorophores is below 10 nm, fluorescent tags positioned C-terminally should restrict FRET to direct neighbors. Modeling also predicted that the C termini extend outside the helix, away from the lateral surfaces of the GCPs, suggesting that the addition of the fluorescent proteins should not interfere with protein-protein interactions

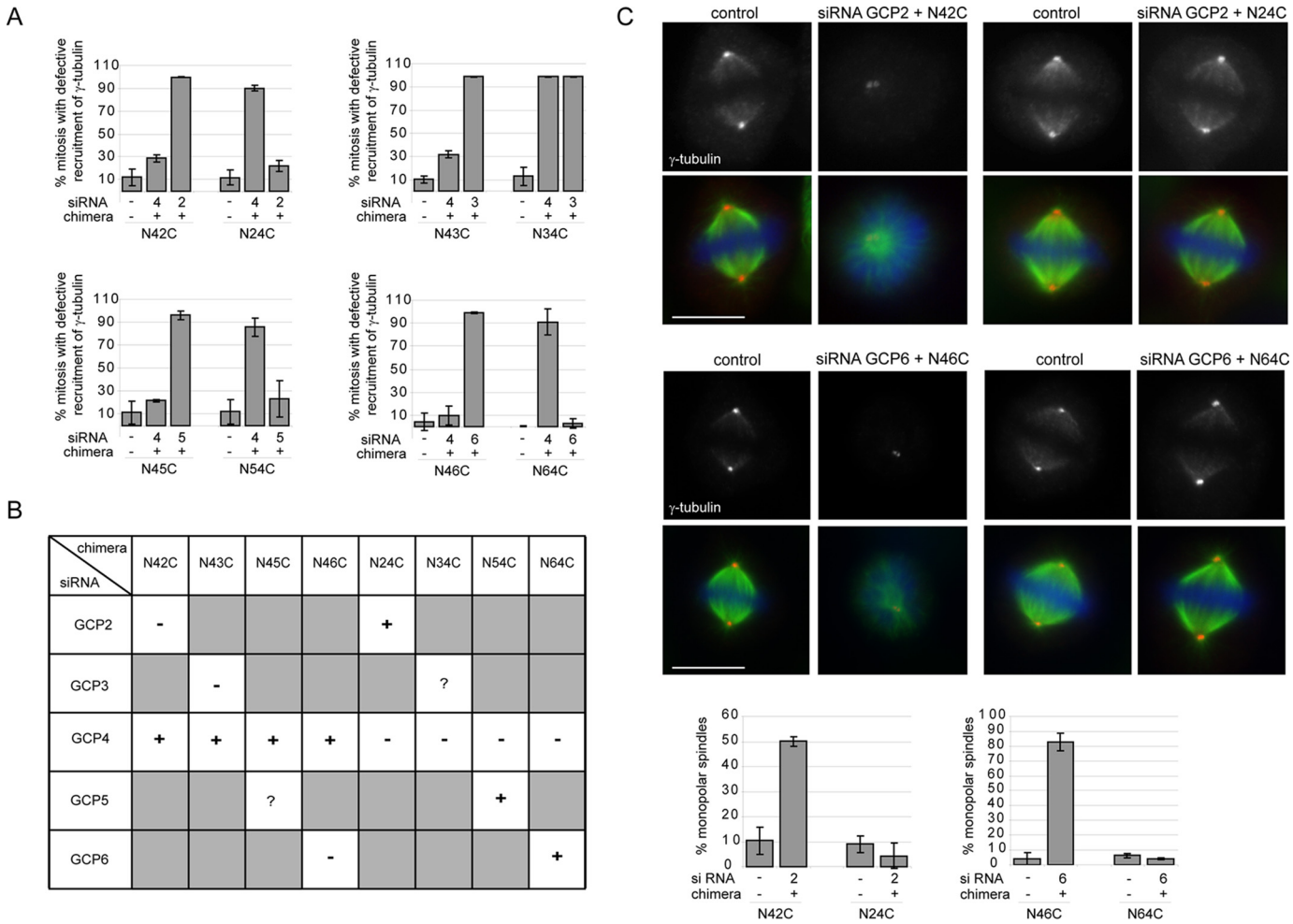


FIGURE 3. **Chimeric GCPs rescue γTuRC recruitment and function, in addition to γTuRC assembly.** *A*, percentage of cells with defective recruitment of γ-tubulin (mean of three experiments, 300 total cells scored per condition). *B*, summary of the function of the chimeras in γTuRC assembly as well as recruitment in mitosis (+, rescue; −, no rescue; ?, ambiguous; *gray squares*, not evaluated). *C*, comparison of mitosis in control cells or siRNA-treated cells with induction of the chimeras, stained for γ-tubulin (*top panels* and *red*), microtubules (*green*), and DNA (*blue*). *Scale bar*, 10 μm. The graphs show the percentage of monopolar spindles. Results are shown for the N42C/N24C and N46C/N64C chimeras treated with siRNAs against GCP2 and GCP6, respectively (mean of three experiments, 300 total cells scored per condition). Because the yield of monopolar spindles is lower after GCP5 siRNA, results for the N45C/N54C chimeras are not shown, nor are they for the N43C/N34C chimeras that are not rescue-competent. *Error bars*, S.E., 95% confidence interval.

and should not inhibit the assembly of the complex. Indeed, the tagged GCPs were recruited to the centrosomal Nlp assemblies, and their presence did not alter microtubule nucleation, indicating that they were functional (Fig. 5*C*).

We first used GCP2 and GCP3 as controls. We fused GFP to the C terminus of GCP3 and mCherry to the C termini of GCP2 and GCP3. Centrosomal assemblies containing GCP3-GFP displayed an average lifetime of 2.414 ns. When co-expressed with GCP2-mCherry, the lifetime decreased to 1.981 ns, but only to 2.293 ns with GCP3-mCherry (Table 1, Fig. 5, *D–F*). This corresponds to FRET efficiencies of 18% for the GCP3/GCP2 pair and 5% for the GCP3/GCP3 pair. For comparison, the use of free mCherry as an acceptor led to 3.7% that of FRET efficiency (Table 1). Only values >7% are considered significant (see "Experimental Procedures" for details). These results are consistent with the existing model of γTuSC helices, with GCP3 in direct contact with GCP2 but with distances between GCP3 C termini exceeding the radius for efficient FRET (Fig. 5, *E* and *F*).

Using GCP4-GFP paired with GCP5-mCherry or GCP5-GFP paired with GCP4-mCherry, we obtained FRET efficiencies between 8 and 9% (Table 1, Fig. 6, *A* and *B*). In contrast, pairing GCP4-GFP with GCP4-mCherry or GCP5-GFP with GCP5-mCherry led to <3% of FRET efficiency (Table 1, Fig. 6*C*). These values are consistent with a close and specific proximity of the C termini of GCP4 and GCP5. Note that FRET is more efficient with the GCP2/GCP3 pair than with the GCP4/GCP5 pair, because GCP3-GFP has the potential to transfer energy simultaneously to two molecules of GCP2-mCherry in the helix, which potentiates the energy transfer (Fig. 5*E*). GCP4 can only have one GCP5 neighbor because there is only one copy of GCP5 per complex (16, 19). To verify that the interaction revealed by FRET is direct as expected, we performed cross-linking experiments *in vitro* on purified γTuRC. Despite the large size and low abundance of the complex, we were able to reveal by Western blot a cross-linked product containing both proteins at the size of the heterodimer (Fig. 6*D*). This confirms that GCP4 and GCP5 are direct neighbors within the complex.

We then used GCP4 and GCP5 fluorescently tagged at their N termini. Again, we measured significant FRET (9.5–12%), in contrast to pairs of one protein tagged at its C terminus and the

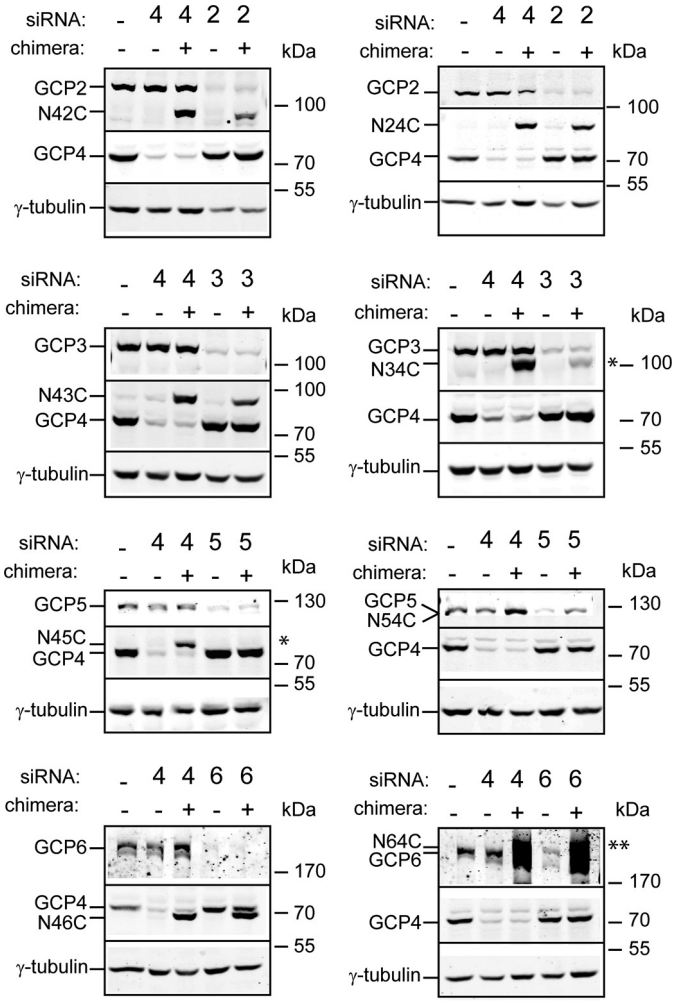


FIGURE 4. **Levels of induction of the chimeric GCPs in the HeLa stable cell lines.** Western blot analysis of extracts from the stable cell lines treated with or without siRNA against GCPs 2, 3, 4, 5, or 6 with or without induction of the chimera. The levels of induction were grossly similar to the levels of the endogenous proteins, except for the chimeras N34C and N45C that were barely detectable after treatment with GCP3 and GCP5 siRNA respectively (*). In contrast, induction of the chimera N64C was around 15× more than the endogenous GCP6 (**).

other at the N terminus (0.5–3.5%) (Table 1, Fig. 7, *A* and *B*). The latter arrangement should not permit FRET if GCPs 4 and 5 were associated in a γTuSC-like manner, in which the N terminus of one GCP is separated by an average distance of 12 nm from the C terminus of the neighboring GCP. Altogether, our combined results provide direct evidence for lateral interaction between GCP4 and GCP5, equivalent to GCPs 2 and 3 in γTuSCs. To test whether the GCP4-GCP5 interaction requires the specific N-terminal domain of each partner, we used the chimeric proteins with the N- and C-terminal domains of GCP4 and GCP5 swapped, tagged C-terminally with GFP. We measured significant FRET between the donor chimera carrying the N-terminal domain of GCP4 and GCP5-mCherry as an acceptor (9%) but not with GCP4-mCherry (4%) (Table 1, Fig. 7, *C* and *D*). Likewise, we measured significant FRET using the chimera carrying the N-terminal domain of GCP5 paired with GCP4-mCherry (8%) but not with GCP5-mCherry (2%) (Table 1, Fig. 7, *E* and *F*). These results confirm the role of the N-terminal domains in the interaction between GCP4 and GCP5.

*Interaction of GCP4 with γ-Tubulin Is Not Necessary for Incorporation into the γTuRC*—Our results show that the C-terminal domains of the GCPs are exchangeable, suggesting that they perform the same function, *i.e.* binding to γ-tubulin. We wanted to address the significance of the GCP/γ-tubulin interaction in γTuRC assembly. For this, we mutated the γ-tubulin binding region of GCP4 and evaluated its function in γTuRC assembly and recruitment along spindles. Based on the models of the GCP4 structure fitted into the reconstruction of γTuSC helices, we predicted the regions of GCP4 involved in the interaction with γ-tubulin (27, 28, 32). Helices α16 and α20 of the C-terminal domain of GCP4 were found at the protein interface with γ-tubulin (Fig. 8*A*). We mutated both helices and evaluated the binding of the mutants to γ-tubulin *in vitro* by isolating stable complexes of FLAG-tagged γ-tubulin and V5-tagged GCP4 on anti-FLAG affinity beads. Multiple mutations in helix α16 inhibited binding of GCP4 to γ-tubulin, whereas mutating helix α20 showed no effect (Fig. 8, *A* and *B*). Refining the mutations revealed that mutating residue Phe-522 of α16 to Arg reduced the binding and that adding the F626R mutation in α20 was fully inhibitory (Fig. 8, *A* and *B*).

We tested the ability of the double mutant F522R/F626R to complement the depletion of the endogenous GCP4. A stable cell line expressing the siRNA-resistant GCP4 F522R/F626R still assembled γTuRCs after siRNA treatment, as shown after sucrose gradient sedimentation, and γ-tubulin was still recruited to the mitotic spindle (Fig. 8, *C–E, upper panels*). In contrast, deletion of the whole C-terminal domain of GCP4 was unable to rescue (Fig. 8, *C–E*, *lower panels*). We observed that GCP4 was present in low density fractions of the sucrose gradients, independent of γTuRCs (Fig. 8*F*). Immunoprecipitation of GCP4 from these fractions indicated a specific interaction with γ-tubulin (Fig. 8*G*). When WT GCP4 was replaced by the double mutant F522R/F626R, the interaction was lost (Fig. 8*H*), confirming that the F522R/F626R mutations inhibited the binding of GCP4 to γ-tubulin not only *in vitro* but also in cells where γTuRC assembly is rescued. Moreover, the lateral association with GCP5 was not altered, as controlled by FLIM-FRET (Table 1). These results indicate that the C-terminal domain of GCP4 is needed for incorporation into the γTuRC, but not the interaction with γ-tubulin.

## Discussion

In this work we provide the first experimental evidence supporting the prediction that all GCPs assemble into the helical wall of the γ-TuRC. Using chimeric proteins formed by the N-terminal domain of one GCP fused to the C-terminal domain of another GCP, we show that the N-terminal domains determine the identity of the GCPs. Moreover, our FLIM-FRET experiments indicate that GCP4 and GCP5 establish γTuSC-like lateral interactions within the complex. Previous studies in *S. pombe* have suggested an interaction between GCP4 and GCP5, independent of the presence of GCP2 and GCP3 (17), and our cross-linking results confirm a direct association of GCP4 and GCP5 within γTuRCs. Using chimeric proteins with the N- or C-terminal domains of GCP4 and 5 swapped, we show that the N-terminal domains carry the specificity of the interaction. Altogether, our results suggest that the N-terminal

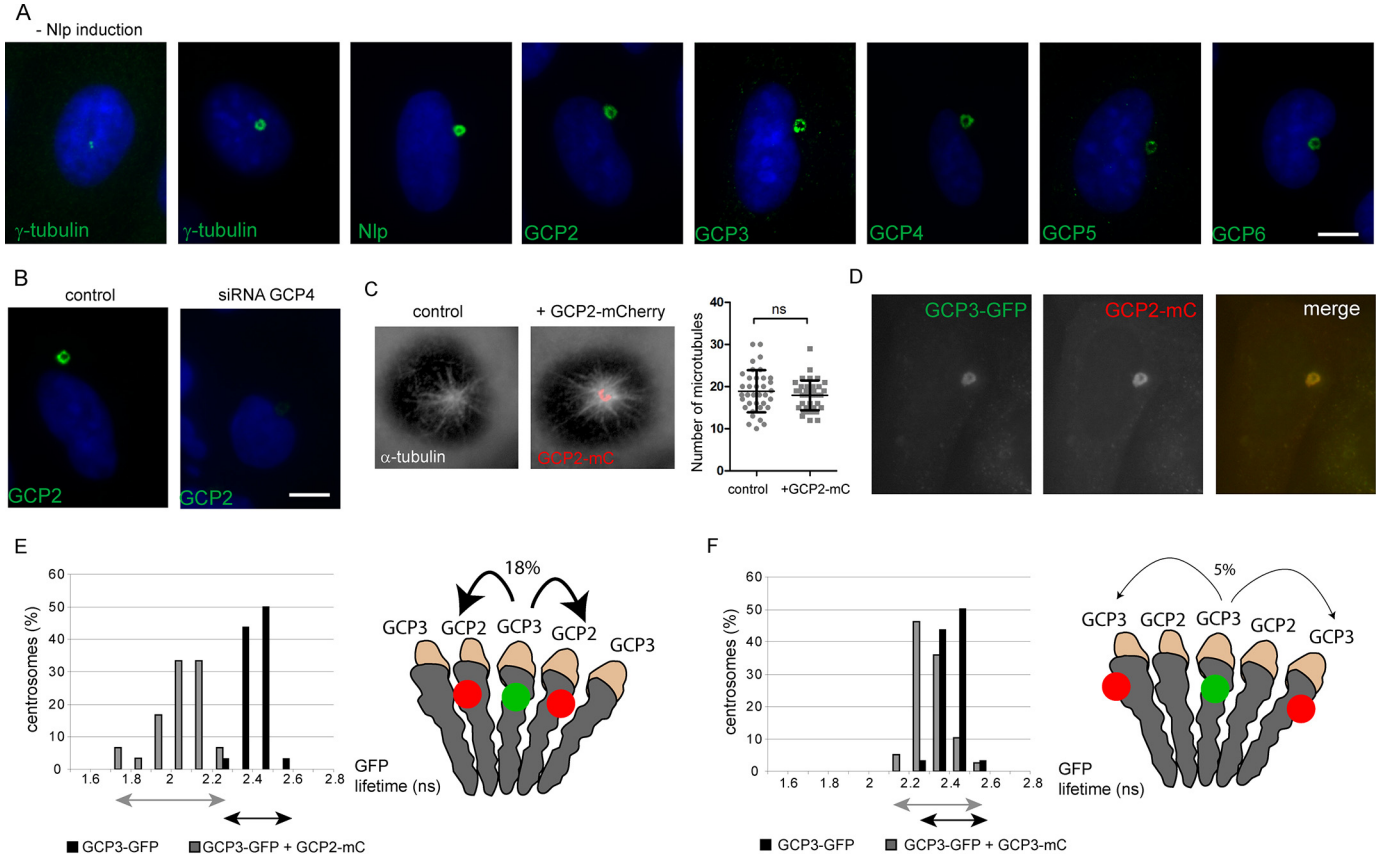


FIGURE 5. **Specific energy transfer between adjacent GCPs within γTuRCs at centrosomal Nlp assemblies.** *A*, localization of γ-tubulin and GCPs in U2OS cells overexpressing Nlp (*left panel*, no induction of Nlp overexpression). *B*, localization of GCP2 in cells overexpressing the Nlp protein with or without treatment with GCP4 siRNA. *C*, microtubule regrowth assay on cells overexpressing the Nlp protein with or without expression of GCP2-mCherry. The graph shows the quantification of the number of microtubules after regrowth (35 cells scored per condition; *error bars*, mean ± S.D.). *D*, localization of GCP3-GFP (*green*) and GCP2-mCherry (*red*) in cells overexpressing Nlp. *E*, GFP lifetime distribution of GCP3-GFP with or without co-expression of GCP2-mCherry. *F*, GFP lifetime distribution of GCP3-GFP with or without co-expression of GCP3-mCherry. Histograms show the percentage of centrosomes according to the lifetime classes. *Schemes on the right* indicate the percentage of FRET efficiency.

domains of all GCPs are mediating specific lateral interactions. Thereby, they define the direct neighbors and position the GCPs within the γTuRC helix.

In addition to the conserved sequences, including the grip1 motif, the N-terminal domains carry specific insertions of various sizes depending on the GCP, *i.e.* internal insertions or N-terminal extensions (27). These insertions may equally contribute to the function of individual GCPs as they have been implied in specific interactions with regulatory or structural proteins. For instance, GCP6 carries a large internal insertion phosphorylated by Plk4 (21) and containing a domain of interaction with keratins (33), whereas the N-terminal extension of GCP3 interacts with the recruitment protein MOZART1 (34, 35).

The N-terminal domains can be fused to C-terminal domains of other GCPs without affecting their function and specificity. This was shown for the N-terminal domains of GCPs 2, 4, 5, and 6 but remains uncertain for GCP3. The poor induction of GCP3 chimera did not allow us to test unambiguously whether it rescues the depletion of the endogenous GCP3. Either the expression level was insufficient for rescuing, or the C-terminal domain of GCP3 was irreplaceable. One difference between GCP3 and the other GCPs is the flexibility of the GCP3 hinge linking the N- and C-terminal domains. This flexibility is needed to close the γTuRC in a conformation compatible with the geometry of the microtubule, increasing its nucleation capacity (11). In the chimera composed of the N-terminal domain of GCP3 and the C-terminal domain of GCP4, the flexibility or the positioning of the C-terminal domain might be altered and impact the assembly of the complex. The observation that the C-terminal domains of all other GCPs can be switched fits with the structural data, which predict an interaction with γ-tubulin via the conserved grip2 motif (27, 32, 36). They could thus be exchangeable if the GCPs were all binding similarly to γ-tubulin. Surprisingly, we have found that a mutant of GCP4 lacking affinity to γ-tubulin was still able to incorporate into γTuRCs and to rescue their assembly. Thus binding to γ-tubulin might not be essential for all GCPs, and low copy number GCPs might participate in γTuRC assembly even if they do not carry their own copy of γ-tubulin. γTuRCs assembled with the mutant GCP4 were recruited to mitotic spindles and did not induce monopolarity, suggesting that they were functional. However, we do not know whether γTuRCs with mutant GCP4 can "fill the gap" by integrating γ-tubulin without longitudinal GCP4 interaction, simply by lateral interactions with neighboring γ-tubulins.

The precise stoichiometry of GCPs 4, 5, and 6 within γTuRCs remains unclear. Co-immunoprecipitation of endogenous

**TABLE 1**
**FLIM-FRET measurements showing a pseudo-TuSC interaction between GCP4 and GCP5**
NA, no acceptor; bold indicates significant FRET efficiency.

| Donor | Acceptor | $\tau^a$ | S.E. | $\Delta\tau^b$ | n$^c$ | FRET$^d$ | $p$ value$^e$ |
|---|---|---|---|---|---|---|---|
| | | *ns* | | *ps* | | *%* | |
| GCP3-GFP | NA | 2.414 | 0.006 | | 121 | | |
| | mCherry | 2.325 | 0.019 | 89 | 29 | 3.7 | $2.5 \times 10^{-8}$ |
| | **GCP2-mC** | **1.981** | **0.026** | **433** | **60** | **17.9** | $\mathbf{2.4 \times 10^{-51}}$ |
| | GCP3-mC | 2.293 | 0.011 | 121 | 128 | 5.0 | $1.4 \times 10^{-19}$ |
| GCP4-GFP | NA | 2.444 | 0.006 | | 123 | | |
| | GCP4-mC | 2.391 | 0.008 | 53 | 97 | 2.2 | $2.5 \times 10^{-7}$ |
| | **GCP5-mC** | **2.251** | **0.013** | **193** | **88** | **7.9** | $\mathbf{3.6 \times 10^{-33}}$ |
| | GCP6-mC | 2.347 | 0.010 | 97 | 90 | 4.0 | $3.6 \times 10^{-2}$ |
| GCP5-GFP | NA | 2.425 | 0.008 | | 136 | | |
| | **GCP4-mC** | **2.213** | **0.015** | **211** | **80** | **8.7** | $\mathbf{9.6 \times 10^{-29}}$ |
| | GCP5-mC | 2.369 | 0.018 | 55 | 50 | 2.3 | $2.0 \times 10^{-3}$ |
| | GCP6-mC | 2.345 | 0.018 | 80 | 57 | 3.3 | $1.0 \times 10^{-5}$ |
| GCP6-GFP | NA | 2.436 | 0.007 | | 152 | | |
| | GCP4-mC | 2.422 | 0.014 | 13 | 60 | 0.6 | $1.6 \times 10^{-1}$ |
| | GCP5-mC | 2.353 | 0.008 | 83 | 60 | 3.4 | $1.6 \times 10^{-1}$ |
| | GCP6-mC | 2.354 | 0.012 | 82 | 44 | 3.4 | $1.7 \times 10^{-7}$ |
| GFP-GCP4 | NA | 2.402 | 0.009 | | 60 | | |
| | GCP5-mC | 2.390 | 0.008 | 12 | 60 | 0.5 | $3.4 \times 10^{-1}$ |
| GFP-GCP5 | NA | 2.409 | 0.022 | | 70 | | |
| | GCP4-mC | 2.326 | 0.022 | 83 | 43 | 3.5 | $2.3 \times 10^{-2}$ |
| GFP-GCP4 | NA | 2.499 | 0.008 | | 60 | | |
| | mC-GCP4 | 2.408 | 0.009 | 91 | 60 | 3.6 | $7.4 \times 10^{-12}$ |
| | **mC-GCP5** | **2.262** | **0.009** | **237** | **60** | **9.5** | $\mathbf{3.3 \times 10^{-37}}$ |
| GFP-GCP5 | NA | 2.460 | 0.009 | | 60 | | |
| | **mC-GCP4** | **2.162** | **0.018** | **298** | **60** | **12.1** | $\mathbf{4.6 \times 10^{-29}}$ |
| | mC-GCP5 | 2.388 | 0.010 | 72 | 60 | 2.9 | $3.5 \times 10^{-7}$ |
| N45C-GFP | NA | 2.473 | 0.009 | | 80 | | |
| | GCP4-mC | 2.377 | 0.009 | 96 | 60 | 3.9 | $5.5 \times 10^{-11}$ |
| | **GCP5-mC** | **2.258** | **0.012** | **215** | **90** | **8.7** | $\mathbf{3.3 \times 10^{-30}}$ |
| N54C-GFP | NA | 2.456 | 0.007 | | 120 | | |
| | **GCP4-mC** | **2.261** | **0.014** | **195** | **60** | **7.9** | $\mathbf{5.2 \times 10^{-32}}$ |
| | GCP5-mC | 2.412 | 0.010 | 44 | 60 | 1.8 | $3.2 \times 10^{-4}$ |
| GCP4(F522R-F626R)-GFP | NA | 2.407 | 0.008 | | 60 | | |
| | **GCP5-mC** | **2.169** | **0.019** | **238** | **60** | **9.9** | $\mathbf{1.5 \times 10^{-20}}$ |

[a] Mean lifetime (in ns).
[b] $\Delta\tau = \tau_D - \tau_{DA}$ (in ps).
[c] Total number of measured centrosomes.
[d] Percentage of FRET efficiency: $E = 1 - (\tau_{DA}/\tau_D)$.
[e] $p$ value of the difference between the donor lifetimes in the presence and absence of acceptor (Student's t test).

GCP4 or GCP5 with tagged forms suggested that more than one copy of GCP4 but only one of GCP5 are present per complex (16). Estimation from gels of purified γTuRCs also suggested an average of 2.5 copies of GCP4, one copy of GCP5 and <1 copy of GCP6 (although GCP6 is essential for γTuRC assembly, this result is still to be confirmed; 19). Because of their low stoichiometry and because they are all essential, we think that GCP 4, 5, and 6 are positioned at specific locations, critical for the formation or stability of the helix. Our limited analysis revealed that the positions of GCP4 and GCP5 were not random and that the two proteins were adjacent within γTuRCs. Experiments in fungi suggest that GCP 4, 5, and 6 might form a subcomplex within γTuRCs (17, 37, 38). We failed to detect an interaction with GCP6 by FLIM-FRET using C-terminally tagged GCP 4, 5, and 6 (see Table 1), suggesting that GCP6 is not laterally associated with GCP4 or GCP5. Alternatively, the wide insertion present in the middle of GCP6 might position its C terminus away from the neighboring protein, preventing FRET. We propose that GCP 4, 5, and 6 position together at the ends of the helix, which would allow them either to initiate or terminate the self-assembly of γTuSCs and/or to stabilize the structure by bridging the two ends. Although several models can be proposed, we favor a model in agreement with our FLIM-FRET results in which GCP4 and -5 interact laterally at one end of the helix and GCP6 is located at the other end. In this configuration, a longitudinal interaction between GCP6 and GCP4/5 might close and stabilize the complex (Fig. 9). Finding the precise positions of GCP 4, 5, and 6 will be essential to understand their contribution to the function of γTuRCs.

## Experimental Procedures

*Plasmid Constructs*—Human GCPs 2, 3, 4, 5, and 6 cDNAs were cloned into pCDNA5/FRT/TO (Invitrogen) using high fidelity PCR with oligonucleotides with tailored restriction sites: GCP2 and GCP3 (39), GCP4 (15), GCP5 (image clone 5297149), and GCP6 (21). Five silent point mutations within the siRNA targeting sequence of the GCPs cDNAs were introduced by PCR to generate resistance. For FLIM-FRET analysis, the sequences of AcGFP and mCherry were added at the 5′ or 3′ end of the GCPs cDNAs by PCR with a linker of six residues (AcGFP/mCherry-AGGGGG-GCP or GCP-GGGGGA-AcGFP/mCherry). Mutations within the C-terminal domain of GCP4 were introduced into the pET26B-GCP4-V5 (27) by PCR. The chimeric constructs were generated by introducing a NheI restriction site at the junction of the N-terminal and C-terminal domains of the GCPs by PCR and by swapping the domains using the sites flanking the constructs in pCDNA5/FRT/TO. For the GCP3 chimera, the domains were also swapped using the Gibson kit (NEB) without introduction of the NheI restriction site.

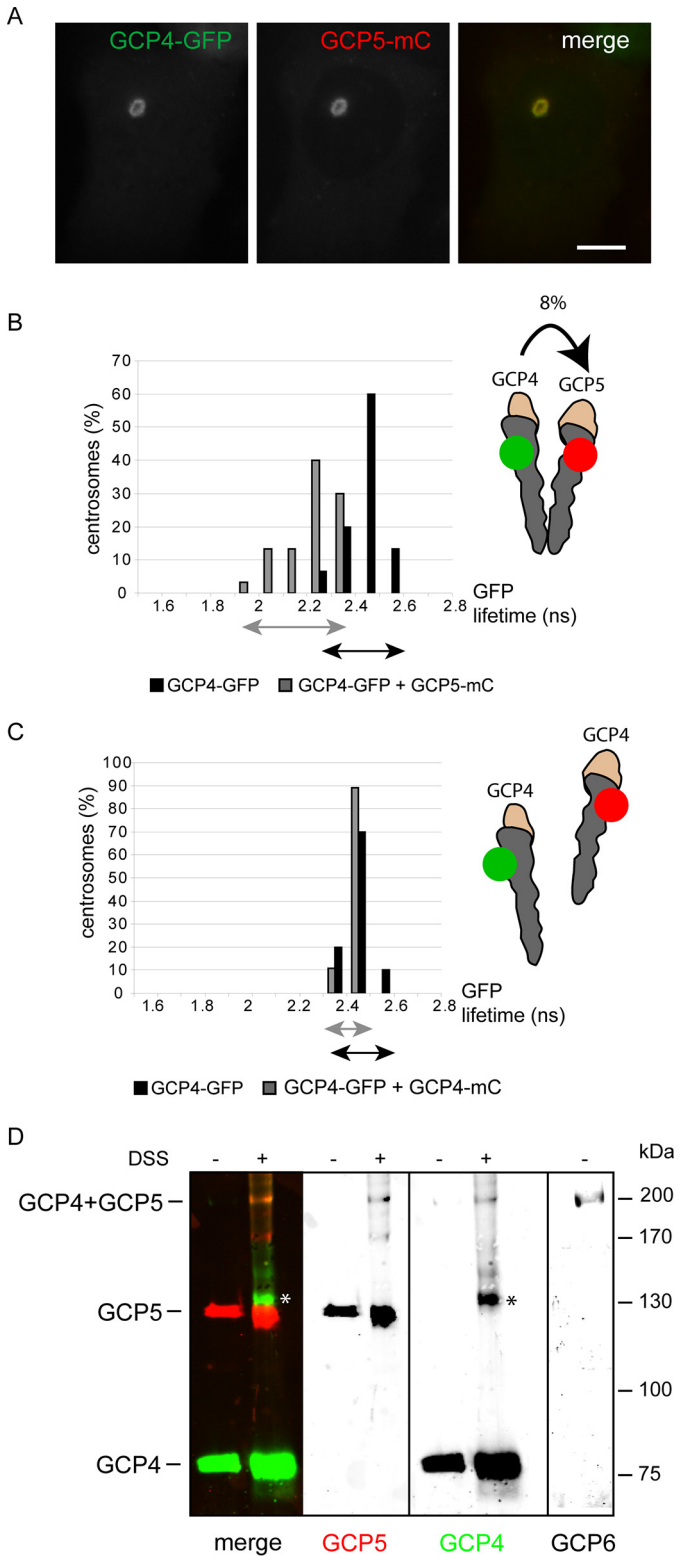


FIGURE 6. **GCP4 and GCP5 interact directly within γTuRCs.** *A*, localization of GCP4-GFP (*green*) and GCP5-mCherry (*red*) in cells overexpressing Nlp. *B*, GFP lifetime distribution of GCP4-GFP with or without co-expression of GCP5-mCherry. *C*, GFP lifetime distribution of GCP4-GFP with or without co-expression of GCP4-mCherry. *D*, Western blot analysis of GCP4 and GCP5 after cross-linking of purified γTuRCs *in vitro*. At low concentration of cross-linker, a specific band containing GCP4 (76 kDa) and GCP5 (118 kDa) appears at the size of GCP6 (used here as a marker of 200 kDa), corresponding to the size of the heterodimer. An additional band containing GCP4 was also observed around 130 kDa (*).

*Cell Culture and Generation of Stable Cell Lines*—HeLa Flp-in T-Rex (a gift from S. Taylor, University of Manchester, UK), U2OS T-Rex Myc Nlp (from E. Nigg, University of Basel, Switzerland), and HeLa S3 γ-tubulin-Myc-TAP (from J. Lüders, IRB Barcelona, Spain) were grown at 37 °C in a 5% $CO_2$ atmosphere in Dulbecco's modified Eagle's medium (DMEM) supplemented with 10% fetal bovine serum (31, 40). HeLa Flp-in T-Rex were cultured with Zeocin (100 μg/ml) and blasticidin (5 μg/ml). The pCDNA5/FRT/TO vectors containing the GCPs cDNAs were co-transfected with the Flp recombinase encoding plasmid pOG44 (Invitrogen) using $CaCl_2$. Hygromycin B-resistant clones (200 μg/ml) were picked and expanded to obtain clonal cell lines. Transgene expression was induced using 1 μg/ml doxycycline. Two independent clones with levels of expression similar to endogenous levels (except for the N64C chimera that was strongly overexpressed) were systematically chosen and analyzed. The results were similar between clones. U2OS T-Rex Myc Nlp were cultured with Zeocin (100 μg/ml) and hygromycin B (50 μg/ml). Nlp overexpression was induced using 1 μg/ml doxycycline. HeLa S3 γ-tubulin-Myc-TAP were cultured with 400 μg/ml Geneticin.

*RNAi and Transfections*—For RNAi, the following sequences were used as targets: GCP2 (5′-GGCUUGACUUCAAUGGUUU-3′), GCP3 (5′-CGAUUAUCAUGUUGACGGA-3′), GCP4 (5′-GCUGCUUCAUCAGAUCAAU-3′), GCP5 (5′-CGUUAUAUAGCGUAUCAGA-3′), GCP6 (5′-GAUGAGACUCAACAGCUGC-3′). Double-stranded siRNA oligomers (Ambion) were transfected using Lipofectamine RNAi max (Invitrogen). Cells were seeded the day before transfection at 600,000 cells in 100-mm Ø dishes (for sucrose gradient experiments) or at 100,000 cells in 6-well dishes on coverslips (for immunofluorescence). 10 nM siRNAs were transfected according to the manufacturer's protocol, and the medium was replaced with or without 1 μg/ml doxycycline after 5 or 24 h. Cells were harvested or fixed 72 h post-transfection. For FRET experiments, 800 ng of plasmid DNA were transfected using Lipofectamine 2000 (Invitrogen) into cells seeded in 24-well dishes on coverslips. Medium was changed after overnight incubation, with 1 μg/ml doxycycline. After 7 h of induction, cells were fixed for 15 min in 4% paraformaldehyde and mounted in Vectashield.

*Sucrose Gradients*—Cells were trypsinized, rinsed with PBS, and resuspended in gradient buffer (50 mM HEPES, pH 7.4, 100 mM KCl, 1 mM EGTA, 1 mM $MgCl_2$, 1 mM GTP, 1 mM DTT) with 1% Nonidet P-40 and complete protease inhibitor mix (Roche Applied Science). After 10 min centrifugation at 16,000 − *g*, soluble extracts were fractionated on gradients of 5–40% sucrose in gradient buffer, in a SW55-Ti Rotor (Beckman coulter) at 50,000 rpm for 4.5 h. Fractions were precipitated in methanol and resuspended in gel loading buffer containing SDS. Proteins were detected by Western blot using the Odyssey imaging system (Li-cor Biosciences), with IRDye 800CW- and 680CW-conjugated secondary antibodies (Invitrogen). γ-Tubulin levels were quantified using the Odyssey 2.1 software: the Odyssey fluorescence system provides a linear relationship between signal intensity and antigen loading. Band intensities were measured with background subtraction, and the values were normalized relative to the total γ-tubulin

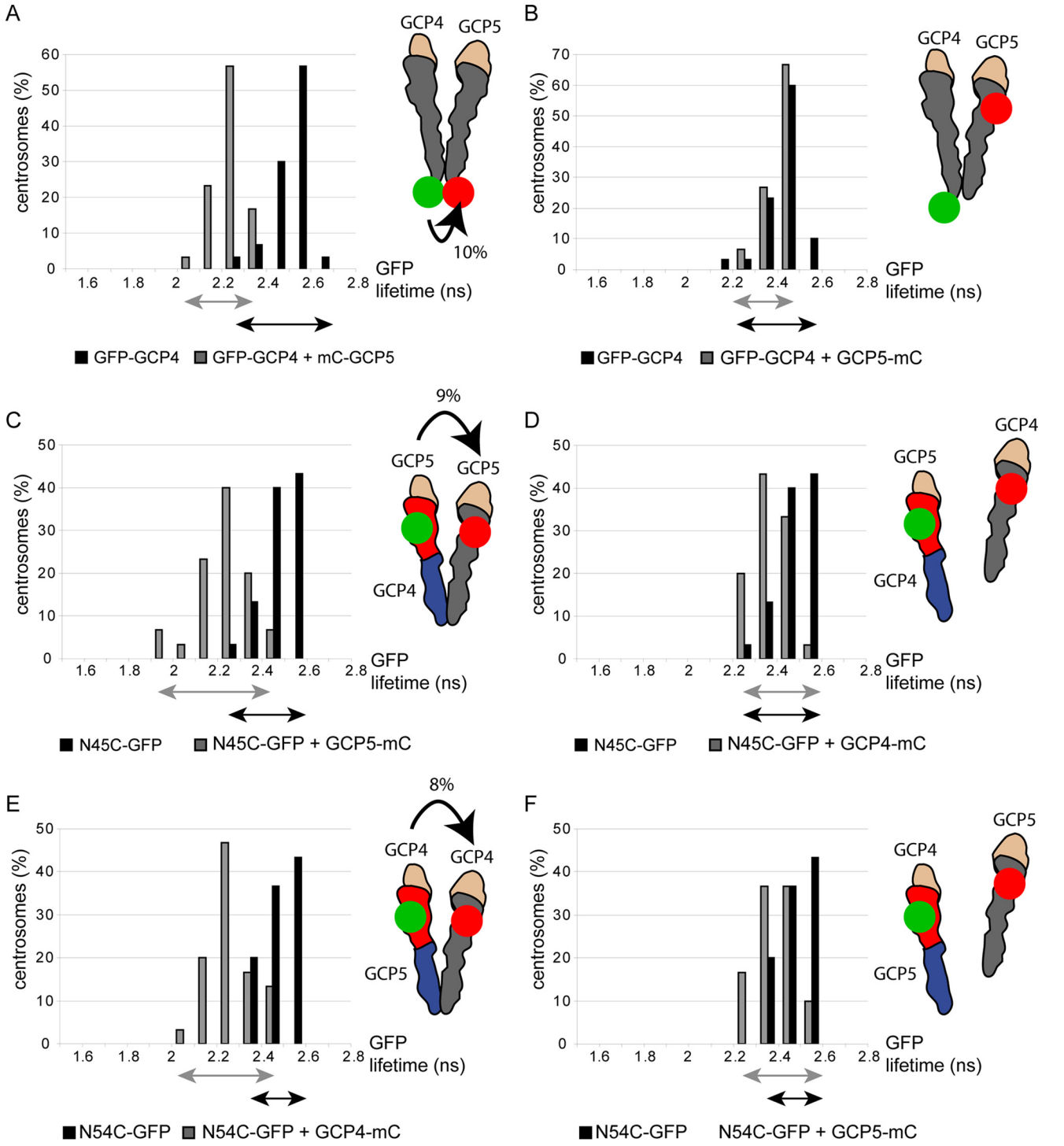


FIGURE 7. **GCP4-GCP5 associate laterally via their N-terminal domains.** *A*, GFP lifetime distribution of GFP-GCP4 with or without co-expression of mCherry-GCP5. *B*, GFP lifetime distribution of GFP-GCP4 with or without co-expression of GCP5-mCherry. *C*, GFP lifetime distribution of N45C-GFP with or without GCP5-mCherry. *D*, GFP lifetime distribution of N45C-GFP with or without GCP4-mCherry. *E*, GFP lifetime distribution of N54C-GFP with or without GCP4-mCherry. *F*, GFP lifetime distribution of N54C-GFP with or without GCP5-mCherry.

amount, corresponding to the sum of the intensities of all the fractions. For immunoprecipitation, gradient fractions were incubated with anti-GCP4 FL antibody for 2 h at 4 °C and with protein A magnetic beads (Dynal) for an additional 2 h. The beads were washed twice in gradient buffer, and samples were eluted in gel loading buffer.

*Cross-linking Experiments*—γTuRCs were purified from a HeLa S3 cell line expressing γ-tubulin-Myc-TAP as described in Teixidó-Travesa *et al.* (40). Purified complexes were cross-linked with 0.5 mM DSS (disuccinimidyl suberate) for 7 min at 20 °C. The cross-linking was stopped by adding 50 mM Tris, pH 8, for 15 min at 4 °C. Cross-linked complexes were analyzed by Western blot after denaturing SDS-PAGE.

*FLAG Pulldown Assay*—FLAG-γ-tubulin and GCP4-V5 (WT and mutants) were transcribed and translated together in a coupled reticulocyte lysate system, according to the manufac-

turer (TNT, Promega), as described in Guillet *et al.* (27). The sample was then incubated with 10 μl of anti-FLAG M2 agarose beads (Sigma) for 2 h at 4 °C and then washed 3 times with 30 μl of HEPES buffer (50 mM HEPES, pH 7.4, 150 mM NaCl, 1 mM EGTA, and 2 mM $MgCl_2$). The bound proteins were eluted by increasing buffer stringency: HEPES 500 (HEPES buffer with 500 mM NaCl), Nonidet P-40 (HEPES buffer supplemented with 1% Igepal CA-630 (Sigma)), radioimmune precipitation

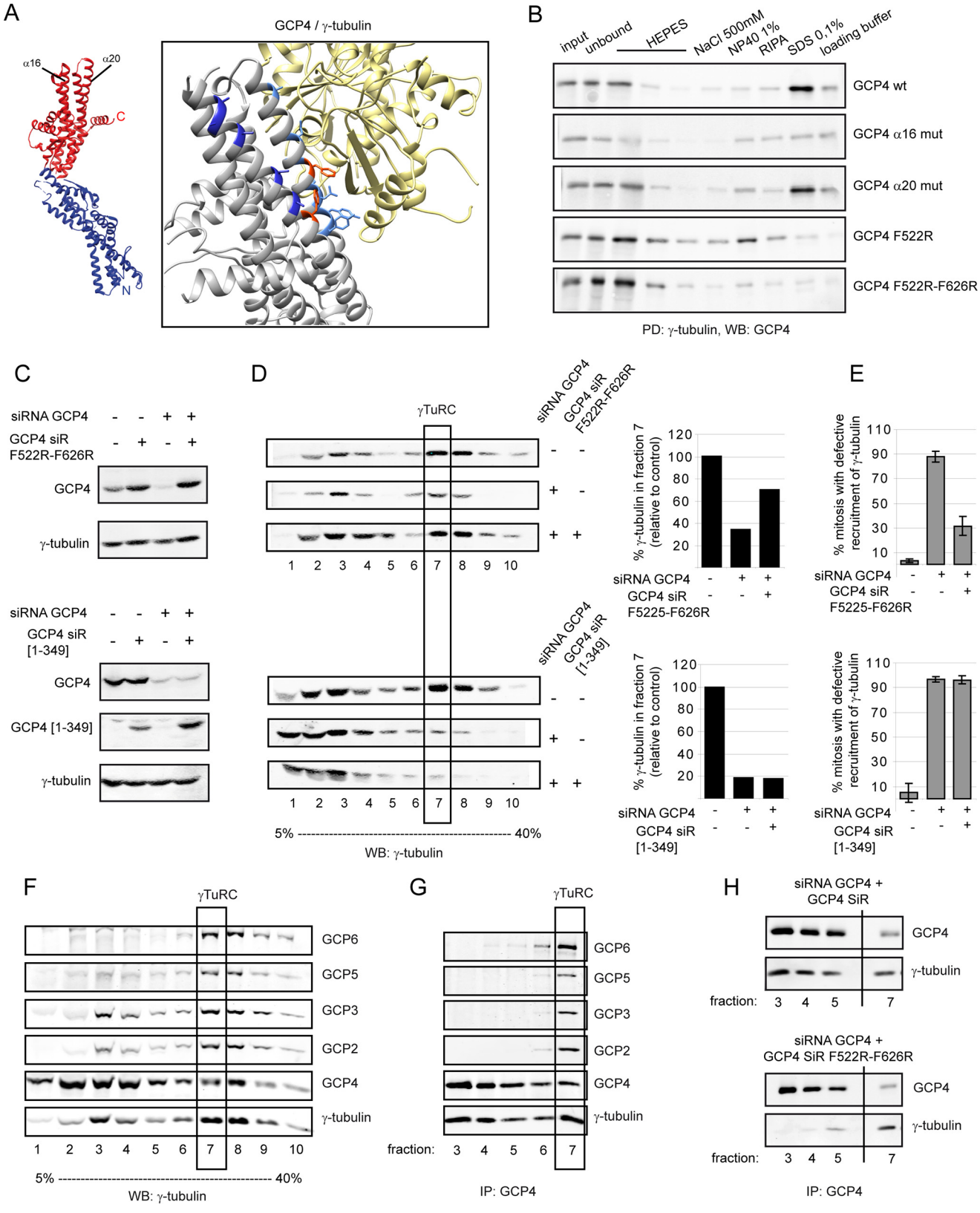

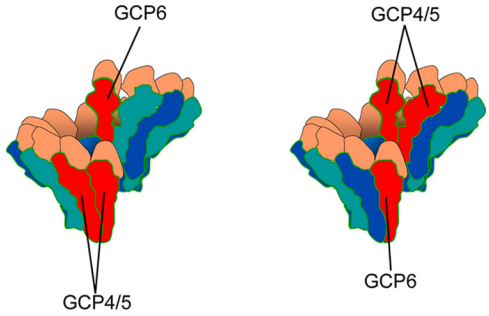


FIGURE 9. **Model of positioning of GCP4, 5, and 6 within γTuRCs.** GCPs 4, 5, and 6 are part of the γTuRC helix, with GCP4 and GCP5 interacting laterally. We propose that they are located at the overlapping ends of the helix, allowing them to initiate or terminate the assembly of the complex. As we have not detected a proximity between the C termini of GCP4/5 and GCP6, we propose that GCP4/5 position at one end of the helix, whereas GCP6 positions at the other end. GCP6 might interact longitudinally with GCP4/5 and bridge the ends of the helix, to stabilize its structure.

assay buffer (HEPES buffer supplemented with 1% Igepal CA-630 and 0.25% deoxycholic acid), SDS (HEPES buffer supplemented with 0.1% SDS), and gel loading buffer containing SDS. Fractions were analyzed by Western blot.

*Antibodies*—The following primary antibodies were used: anti-α-tubulin, mouse (Sigma); anti-γ-tubulin, mouse TU-30 (Exbio) or rabbit R75 (41); anti-GCP2, rabbit (23); anti-GCP3, mouse C3 (Santa Cruz); anti GCP4, rabbit (15); anti-GCP5, rabbit H300 or mouse E1 (Santa-Cruz); anti-GCP6, rabbit (Abcam) or mouse H9 (Santa-Cruz); anti-MYC, mouse (Sigma).

*Immunofluorescence*—Cells grown on coverslips were fixed in −20 °C methanol and processed for immunofluorescence following conventional protocols. For detection, secondary antibodies conjugated to Alexa 488 or 568 (Invitrogen) were used. Fluorescence microscopy was performed on a widefield microscope (Axiovert 200 M; Carl Zeiss MicroImaging, Inc.) equipped with a Z motor using a 40× (Plan Neofluar, 1.3 NA) or 63× (Plan Apo, 1.4 NA) objective. Images were acquired with a MRm camera and Axiovision software (Carl Zeiss MicroImaging, Inc.). Image processing was done using Adobe Photoshop. Quantification of fluorescence was done using Axiovision; intensities at centrosomes and along spindle microtubules were measured on images acquired under constant exposure, within circular areas of 2 μm Ø. An adjacent area of the same dimension was quantified and subtracted as background. For microtubule regrowth, cells were transferred into pre-cooled medium on ice for 1 h and then 15 s into prewarmed medium at 37 °C. Regrowth was stopped by methanol fixation at −20 °C. For all the quantifications, error bars correspond to confidence interval calculated for a probability of 95% (1.96 × S.E.).

*Fluorescence Lifetime*—For FLIM, the light source was a mode-locked Ti:sapphire laser (Tsunami, model 3941, Spectra-Physics) pumped by a 10-watt diode laser (Millennia Pro, Spectra-Physics) and delivering ultrafast femtosecond pulses of light with a fundamental frequency of 80MHz. A pulsepicker (model 3980, Spectra-Physics) was used to reduce the repetition rate to 2 MHz to satisfy the requirements of the triggering unit (working at 2 MHz) and to avoid exposition of the specimen to unwanted excitation pulses. All the experiments were carried out at λ = 850 nm, the optimal wavelength to excite GFP in multiphoton mode (12). All images were acquired with a 60× lens (Plan Apo, 1.4 NA, IR) mounted on an inverted microscope (Eclipse TE2000E, Nikon, Japan) coupled to the FLIM system. In this setup the femtosecond-pulsed laser light is scanned into the left camera port of the microscope via a dichroic mirror (λ < 750 nm). The fluorescence emission is directed back into the detection unit through the same camera port and selected by a band pass filter (520/25 nm). Briefly, the FLIM unit is composed of two galvo mirrors, scanning along the *x* and *y* axes, a relay lens, and a streak camera (Streakscope C4334, Hamamatsu Photonics, Japan) coupled to a fast and high sensitivity CCD camera (model C8800-53C, Hamamatsu). Fluorescence decays were recorded during a time interval of 20 ns. A 4 × 4 binning was used to reduce the acquisition time. The MCP-PMT gain and the exposure time of the CCD were adjusted to avoid overexposure of the CCD. For each image, average fluorescence decay profiles were calculated, and the lifetimes were estimated by fitting these data with a mono- or bi-exponential function using the Levenberg-Marquart non-linear least squares estimation procedure. FRET efficiency was calculated by $E = 1 - (\tau_{DA})/(\tau_D)$, with $\tau_{DA}$ and $\tau_D$ the mean lifetime of the donor in the presence or absence of the acceptor, respectively. Statistical comparisons were performed by Student's *t* test. The relation between the FRET efficiency and the distance *r* between the donor and the acceptor is given by equation $E = 1/(r/R_0)^6$, with $R_0$ the Förster distance to obtain 50% of FRET. Based on the Förster theory, if the distance *r* is $>1.5R_0$, no energy transfer occurs. Taking into account the GFP-mCherry couple of donor and acceptor, we obtained a value close to 7%, meaning that FRET is considered significant only above this value.

*Miscellaneous*—Molecular graphics were performed with the UCSF Chimera package. Chimera is developed by the Resource

FIGURE 8. **The C-terminal domain of GCP4, but not the interaction with γ-tubulin, is necessary to rescue γTuRC assembly.** *A*, ribbon view of GCP4 and representation of the GCP4/γ-tubulin interface modeled by fitting the GCP4 atomic structure into the *S. cerevisiae* γTuSC helix. Mutated residues within helices α16 are colored in *light blue* and within α20 are in *dark blue*. Phe-522 and Phe-626 are colored in *orange*. *B*, pulldown (*PD*) assays using γ-tubulin-FLAG as bait with GCP4 mutants (α16 mut: A511Q, N518R, A521E, F522W, D525R, N526F, Y529R, Y530A; α20 mut: A608W, A609R, S612E, S619W, S623Y). Shown are Western blots (*WB*) of eluted fractions from beads rinsed with HEPES buffer followed by consecutive treatments with 0.5 M NaCl, 0.1% Nonidet P-40, radioimmune precipitation assay buffer, 0.1% SDS, and gel loading buffer, probed with antibody against GCP4. *C*, Western blot analysis of expression of the F522R/F626R GCP4 and the 1–349 truncated GCP4 siR mutants in HeLa cells with or without depletion of the endogenous protein and induction of the mutant. γ-Tubulin is shown as a loading control. *D*, sucrose gradient fractionation of soluble cell extracts. γTuRC sedimentation is visualized using antibody against γ-tubulin. Quantifications of γ-tubulin levels in fraction 7 are shown on the *right*. *E*, percentage of cells with defective recruitment of γ-tubulin (mean of 3 independent experiments, 300 total cells scored per condition). *Error bars*: S.E., 95% CI. *F*, sucrose gradient fractionation of a soluble extract showing GCP4 species in small fractions in addition to γTuRCs. *G*, immunoprecipitation (*IP*) of GCP4 from fractions 3–7 of the gradient. Fraction 3 contains the majority of γTuSCs, and fraction 7 contains γTuRCs. *H*, immunoprecipitation of GCP4 after fractionation of soluble extracts from stable cell lines expressing GCP4 siR WT or F522R/F626R and depleted of the endogenous GCP4. γ-Tubulin is co-precipitated with GCP4 WT in fractions 3–5 but not with GCP4 F522R/F626R, although it is always co-precipitated from γTuRCs in fraction 7.

for Biocomputing, Visualization, and Informatics at the University of California, San Francisco (supported by NIGMS, National Institutes of Health Grant P41-GM103311). PDB structures used were 3RIP for GCP4 atomic structure and 5FLZ for the interface between GCP4 and γ-tubulin.

*Author Contributions*—A. M. and L. H. conceived and coordinated the study and wrote the paper. L. H. designed, performed and analyzed the rescue experiments shown in Figs. 1 and 7. D. F. designed, performed, and analyzed the experiments shown in Figs. 2–6. A. J. carried out the FLIM-FRET measurements and analysis. C C. helped in the construction of vectors of expression of GCPs and performed the pulldown assays in Fig. 7. M.-H. R. designed the GCP4 mutants in Fig. 7. M. C. set up the conditions for Western blot and immunoprecipitation.

*Acknowledgments—We thank S. Jackson, E. Nigg and J. Lüders for providing cell lines, I. Hoffmann and T. Stearns for cDNAs of GCPs, L. Emorine, V. Guillet, L. Mourey, and S. Tournier for helpful discussions, and Ismaïla Li for technical help.*

## References

1. Kollman, J. M., Merdes, A., Mourey, L., and Agard, D. A. (2011) Microtubule nucleation by γ-tubulin complexes. *Nat. Rev. Mol. Cell Biol.* **12,** 709–721
2. Teixidó-Travesa, N., Roig, J., and Lüders, J. (2012) The where, when, and how of microtubule nucleation: one ring to rule them all. *J. Cell Sci.* **125,** 4445–4456
3. Remy, M. H., Merdes, A., and Gregory-Pauron, L. (2013) Assembly of γ-tubulin ring complexes: implications for cell biology and disease. *Prog. Mol. Biol. Transl. Sci.* **117,** 511–530
4. Zheng, Y., Wong, M. L., Alberts, B., and Mitchison, T. (1995) Nucleation of microtubule assembly by a γ-tubulin-containing ring complex. *Nature* **378,** 578–583
5. Moritz, M., Braunfeld, M. B., Sedat, J. W., Alberts, B., and Agard, D. A. (1995) Microtubule nucleation by γ-tubulin-containing rings at the centrosome. *Nature* **378,** 638–640
6. Moritz, M., Braunfeld, M. B., Guénebaut, V., Heuser, J., and Agard, D. A. (2000) Structure of the γ-tubulin ring complex: a template for microtubule nucleation. *Nat. Cell Biol.* **2,** 365–370
7. Oegema, K., Wiese, C., Martin, O. C., Milligan, R. A., Iwamatsu, A., Mitchison, T. J., and Zheng, Y. (1999) Characterization of two related *Drosophila* γ-tubulin complexes that differ in their ability to nucleate microtubules. *J. Cell Biol.* **144,** 721–733
8. Gunawardane, R. N., Martin, O. C., Cao, K., Zhang, L., Dej, K., Iwamatsu, A., and Zheng, Y. (2000) Characterization and reconstitution of *Drosophila* γ-tubulin ring complex subunits. *J. Cell Biol.* **151,** 1513–1524
9. Kollman, J. M., Zelter, A., Muller, E. G., Fox, B., Rice, L. M., Davis, T. N., and Agard, D. A. (2008) The structure of the γ-tubulin small complex: implications of its architecture and flexibility for microtubule nucleation. *Mol. Biol. Cell* **19,** 207–215
10. Kollman, J. M., Polka, J. K., Zelter, A., Davis, T. N., and Agard, D. A. (2010) Microtubule nucleating γ-TuSC assembles structures with 13-fold microtubule-like symmetry. *Nature* **466,** 879–882
11. Kollman, J. M., Greenberg, C. H., Li, S., Moritz, M., Zelter, A., Fong, K. K., Fernandez, J.-J., Sali, A., Kilmartin, J., Davis, T. N., and Agard, D. A. (2015) Ring closure activates yeast γ-TuRC for species-specific microtubule nucleation. *Nat. Struct. Mol. Biol.* **22,** 132–137
12. Lin, T. C., Neuner, A., Schlosser, Y. T., Scharf, A. N., Weber, L., and Schiebel, E. (2014) Cell-cycle dependent phosphorylation of yeast pericentrin regulates γ-TuSC-mediated microtubule nucleation. *Elife* **3,** e02208
13. Lyon, A. S., Morin, G., Moritz, M., Yabut, K. C., Vojnar, T., Zelter, A., Muller, E., Davis, T. N., and Agard, D. A. (2016) Higher-order oligomerization of Spc110p drives γ-tubulin ring complex assembly. *Mol. Biol. Cell* **27,** 2245–2258
14. Erlemann, S., Neuner, A., Gombos, L., Gibeaux, R., Antony, C., and Schiebel, E. (2012) An extended γ-tubulin ring functions as a stable platform in microtubule nucleation. *J. Cell Biol.* **197,** 59–74
15. Fava, F., Raynaud-Messina, B., Leung-Tack, J., Mazzolini, L., Li, M., Guillemot, J. C., Cachot, D., Tollon, Y., Ferrara, P., and Wright, M. (1999) Human 76p: a new member of the γ-tubulin-associated protein family. *J. Cell Biol.* **147,** 857–868
16. Murphy, S. M., Preble, A. M., Patel, U. K., O'Connell, K. L., Dias, D. P., Moritz, M., Agard, D., Stults, J. T., and Stearns, T. (2001) GCP5 and GCP6: two new members of the human γ-tubulin complex. *Mol. Biol. Cell* **12,** 3340–3352
17. Anders, A., Lourenço, P. C., and Sawin, K. E. (2006) Noncore components of the fission yeast γ-tubulin complex. *Mol. Biol. Cell* **17,** 5075–5093
18. Vérollet, C., Colombié, N., Daubon, T., Bourbon, H. M., Wright, M., and Raynaud-Messina, B. (2006) *Drosophila melanogaster* γ-TuRC is dispensable for targeting γ-tubulin to the centrosome and microtubule nucleation. *J. Cell Biol.* **172,** 517–528
19. Choi, Y. K., Liu, P., Sze, S. K., Dai, C., and Qi, R. Z. (2010) CDK5RAP2 stimulates microtubule nucleation by the γ-tubulin ring complex. *J. Cell Biol.* **191,** 1089–1095
20. Izumi, N., Fumoto, K., Izumi, S., and Kikuchi, A. (2008) GSK-3beta regulates proper mitotic spindle formation in cooperation with a component of the γ-tubulin ring complex, GCP5. *J. Biol. Chem.* **283,** 12981–12991
21. Bahtz, R., Seidler, J., Arnold, M., Haselmann-Weiss, U., Antony, C., Lehmann, W. D., and Hoffmann, I. (2012) GCP6 is a substrate of Plk4 and required for centriole duplication. *J. Cell Sci.* **125,** 486–496
22. Scheidecker, S., Etard, C., Haren, L., Stoetzel, C., Hull, S., Arno, G., Plagnol, V., Drunat, S., Passemard, S., Toutain, A., Obringer, C., Koob, M., Geoffroy, V., Marion, V., Strähle, U., *et al.* (2015) Mutations in TUBGCP4 alter microtubule organization via the γ-tubulin ring complex in autosomal-recessive microcephaly with chorioretinopathy. *Am. J. Hum. Genet.* **96,** 666–674
23. Haren, L., Remy, M. H., Bazin, I., Callebaut, I., Wright, M., and Merdes, A. (2006) NEDD1-dependent recruitment of the γ-tubulin ring complex to the centrosome is necessary for centriole duplication and spindle assembly. *J. Cell Biol.* **172,** 505–515
24. Lüders, J., Patel, U. K., and Stearns, T. (2006) GCP-WD is a γ-tubulin targeting factor required for centrosomal and chromatin-mediated microtubule nucleation. *Nat. Cell Biol.* **8,** 137–147
25. Chinen, T., Liu, P., Shioda, S., Pagel, J., Cerikan, B., Lin, T.-C., Gruss, O., Hayashi, Y., Takeno, H., Shima, T., Okada, Y., Hayakawa, I., Hayashi, Y., Kigoshi, H., Usui, T., and Schiebel, E. (2015) The γ-tubulin-specific inhibitor gatastatin reveals temporal requirements of microtubule nucleation during the cell cycle. *Nat. Commun.* **6,** 8722
26. Zhang, L., Keating, T. J., Wilde, A., Borisy, G. G., and Zheng, Y. (2000) The role of Xgrip210 in γ-tubulin ring complex assembly and centrosome recruitment. *J. Cell Biol.* **151,** 1525–1536
27. Guillet, V., Knibiehler, M., Gregory-Pauron, L., Remy, M.-H., Chemin, C., Raynaud-Messina, B., Bon, C., Kollman, J. M., Agard, D. A., Merdes, A., and Mourey, L. (2011) Crystal structure of γ-tubulin complex protein GCP4 provides insight into microtubule nucleation. *Nat. Struct. Mol. Biol.* **18,** 915–919
28. Greenberg, C. H., Kollman, J., Zelter, A., Johnson, R., MacCoss, M. J., Davis, T. N., Agard, D. A., and Sali, A. (2016) Structure of γ-tubulin small complex based on a cryo-EM map, chemical cross-links, and a remotely related structure. *J. Struct. Biol.* **194,** 303–310
29. Gunawardane, R. N., Martin, O. C., and Zheng, Y. (2003) Characterization of a new γTuRC subunit with WD repeats. *Mol. Biol. Cell* **14,** 1017–1026
30. Choy, R. M., Kollman, J. M., Zelter, A., Davis, T. N., and Agard, D. A. (2009) Localization and orientation of the γ-tubulin small complex components using protein tags as labels for single particle EM. *J. Struct. Biol.* **168,** 571–574
31. Casenghi, M., Meraldi, P., Weinhart, U., Duncan, P. I., Körner, R., and Nigg, E. A. (2003) Polo-like kinase 1 regulates Nlp, a centrosome protein involved in microtubule nucleation. *Dev. Cell* **5,** 113–125
32. Cala, O., Remy, M. H., Guillet, V., Merdes, A., Mourey, L., Milon, A., and Czaplicki, G. (2013) Virtual and biophysical screening targeting the γ-tu-

bulin complex: a new target for the inhibition of microtubule nucleation. *PLoS ONE* **8,** e63908

33. Oriolo, A. S., Wald, F. A., Canessa, G., and Salas, P. J. (2007) GCP6 binds to intermediate filaments: a novel function of keratins in the organization of microtubules in epithelial cells. *Mol. Biol. Cell* **18,** 781–794
34. Janski, N., Masoud, K., Batzenschlager, M., Herzog, E., Evrard, J.-L., Houlné, G., Bourge, M., Chabouté, M.-E., and Schmit, A. C. (2012) The GCP3-interacting proteins gip1 and gip2 are required for γ-tubulin complex protein localization, spindle integrity, and chromosomal stability. *Plant Cell* **24,** 1171–1187
35. Dhani, D. K., Goult, B. T., George, G. M., Rogerson, D. T., Bitton, D. A., Miller, C. J., Schwabe, J. W., and Tanaka, K. (2013) Mzt1/Tam4, a fission yeast MOZART1 homologue, is an essential component of the γ-tubulin complex and directly interacts with GCP3(Alp6). *Mol. Biol. Cell* **24,** 3337–3349
36. Suri, C., Joshi, H. C., and Naik, P. K. (2015) Molecular modeling reveals binding interface of γ-tubulin with GCP4 and interactions with noscapinoids. *Proteins* **83,** 827–8243
37. Xiong, Y., and Oakley, B. R. (2009) *In vivo* analysis of the functions of γ-tubulin-complex proteins. *J. Cell Sci.* **122,** 4218–4227
38. Masuda, H., and Toda, T. (2016) Synergistic role of fission yeast Alp16GCP6 and Mzt1MOZART1 in γ-tubulin complex recruitment to mitotic spindle pole bodies and spindle assembly. *Mol. Biol. Cell* **27,** 1753–1763
39. Murphy, S. M., Urbani, L., and Stearns, T. (1998) The mammalian γ-tubulin complex contains homologues of the yeast spindle pole body components spc97p and spc98p. *J. Cell Biol.* **141,** 663–674
40. Teixidó-Travesa, N., Villén, J., Lacasa, C., Bertran, M. T., Archinti, M., Gygi, S. P., Caelles, C., Roig, J., and Lüders, J. (2010) The γTuRC revisited: a comparative analysis of interphase and mitotic human γTuRC redefines the set of core components and identifies the novel subunit GCP8. *Mol. Biol. Cell* **21,** 3963–3972
41. Julian, M., Tollon, Y., Lajoie-Mazenc, I., Moisand, A., Mazarguil, H., Puget, A., and Wright, M. (1993) γ-Tubulin participates in the formation of the midbody during cytokinesis in mammalian cells. *J. Cell Sci.* **105,** 145–156